Melting of $c\bar{c}$ and $b\bar{b}$ pairs in the pre-equilibrium stage of proton-nucleus collisions at the Large Hadron Collider

Lucia Oliva,[1,2,*] Gabriele Parisi,[1,3,†] Vincenzo Greco,[1,3,‡] and Marco Ruggieri[1,2,§]

[1]*Department of Physics and Astronomy "Ettore Majorana," University of Catania, Via Santa Sofia 64, I-95123 Catania, Italy*

[2]*INFN-Sezione di Catania, Via Santa Sofia 64, I-95123 Catania, Italy*

[3]*INFN-Laboratori Nazionali del Sud, Via Santa Sofia 62, I-95123 Catania, Italy*

(Received 11 April 2025; accepted 5 June 2025; published 2 July 2025)

We study the melting of $c\bar{c}$ and $b\bar{b}$ pairs in the early stage of high-energy proton-nucleus collisions. We describe the early stage in terms of an evolving $SU(3)$ glasma stage, that is dominated by intense, out-of-equilibrium gluon fields. On top of these fields, we liberate heavy quark-antiquark pairs, whose constituents are let evolve according to relativistic kinetic theory coupled to the gluon fields. We define a pair-by-pair probability that the pair melts during the evolution, which we relate to the fluctuations of the color charges induced by the interaction of the quarks with the gluon fields. We find that color decorrelation is the main melting mechanism within the pre-equilibrium stage. Moreover, we estimate that within $\Delta\tau \approx 0.4$–0.5 fm/c after the formation time of the pairs, about 50% of $c\bar{c}$ and $b\bar{b}$ pairs are melted.

DOI: 10.1103/nc3z-vns9

I. INTRODUCTION

Relativistic heavy-ion collisions, as performed at the Relativistic Heavy Ion Collider (RHIC) at Brookhaven National Laboratory and at the Large Hadron Collider (LHC) at CERN, provide a unique opportunity to investigate quantum chromodynamics (QCD) at extreme temperatures and densities. Over the past few decades, many experimental results indicated the emergence of a new state of matter, referred to as the quark-gluon plasma (QGP), which forms within $\sim$1 fm/c after the collision and in which quarks and gluons behave as a hydrodynamic fluid of small $\eta/s \sim 0.1$ [1–4]. Such facilities are able to perform measurements also in smaller collision systems such as proton-proton (pp) and proton-nucleus (pA) [5], and these have shown very similar features as those found in heavy ion collisions. While calculations within the hydrodynamic framework have been quite successful in describing observables in these small collision systems, the applicability of hydrodynamics becomes increasingly doubtful as the system size decreases and gradients increase [6,7]. It is also likely that both initial intrinsic momentum correlations and a hydrolike anisotropic expansion are necessary to understand the elliptic anisotropic emission in pA [8–13].

For this reason, a thorough treatment of the initial stages is even more important for pA collisions, and the classical Yang-Mills (CYM) theory offers a good framework for the study of this stage. In fact, CYM well describes the out-of-equilibrium evolution of the highly occupied gluonic system, named the glasma [14], that serves as the initial condition for the system produced in the collisions. The glasma is based on the color-glass-condensate (CGC) effective theory, which stands as a valid description of high-energy nuclei [15–17]; see [18–21] for reviews. The glasma initial condition has been widely used to establish the initial conditions for the subsequent hydrodynamic evolution [22,23].

Heavy quarks (HQs), i.e., charm, c, and beauty, b, represent a unique probe of the early stage of high-energy collisions as well as of the transport properties of the thermalized medium subsequently produced [24–65]. Indeed, due to the large masses, the HQs have a very short formation time of the order of 0.1 fm/c. Therefore the HQ final states, the heavy-flavored hadrons, maintain imprint of the evolution dynamics during the whole collision time frame, with traces from both the initial stage and the subsequent QGP phase. Besides studies on the diffusion of HQs in the QGP and on their hadronization in relativistic nuclear collisions, several works have investigated the impact of the early stage on heavy quarks [66–84]. These have shown that heavy quarks undergo significant diffusion in the early stage, suggesting an impact on experimental

*Contact author: lucia.oliva@dfa.unict.it
†Contact author: gabriele.parisi@dfa.unict.it
‡Contact author: greco@lns.infn.it
§Contact author: marco.ruggieri@dfa.unict.it

observables such as the nuclear modification factor and the elliptic flow, as analyzed in [68]. Since for small systems the thermalized QGP stage is short lived or even absent, HQs could keep a cleaner trace of the early stage with respect to nucleus-nucleus reactions. Thus, for pA collisions the impact of the initial glasma state on final heavy-quark observables may be predominant in the whole evolution of the collision event.

A natural extension of the aforementioned works is to look at the impact of the gluon-dominated initial state on the evolution and dissociation of heavy quarkonia, which are bound states of heavy quarks and antiquarks of the same flavour, namely charmonium $c\bar{c}$ and bottomonium $b\bar{b}$. The production and suppression of heavy quarkonium states in hadronic collisions and in particular in QGP has been widely studied for almost four decades [35,85–110]. In particular, the melting emerges from the interplay of several mechanisms, coming from the different phases of the collision, from initial HQ pair production through the QGP stage to final hadronization, see Refs. [111,112] for a review. As in the QGP, $c\bar{c}$ and $b\bar{b}$ pairs can dissociate also in the evolving glasma [113], with important implications for their evolution in the ensuing QGP medium and for the determination of the heavy-flavored final states produced at hadronization (both open heavy-flavor hadrons and regenerated quarkonia). In the evolving glasma, it is the HQ interaction with the classical color fields that leads to a modification of their spatial and momentum coordinates as well as of their color charge, thus affecting the probability that they survive to the pre-equilibrium stage and enter into the possibly formed QGP phase as a pair.

In this article, we investigate the melting of $c\bar{c}$ and $b\bar{b}$ pairs during the pre-equilibrium stage of high-energy pA collisions, the latter being modeled within the glasma framework. The primary objective of this work is to determine the fraction of pairs that dissociate during the propagation in the evolving glasma, aiming also at disentangling the role of color-charge decorrelation of the HQ pair in the melting, which was only partly addressed before. Within our model the HQs in each pair, formed at $\tau = \tau_{\rm form}$, couple to the strong gluon fields via the Wong equations [114,115] as it has been done in [113]. With respect to the approach presented in [113], we implement a different criterion for the calculation of the number of melting pairs, based on a survival probability, $\mathcal{P}_{\rm survival}$, that takes into account the decorrelation of the color charges induced by the interactions of Q and $\bar{Q}$ with the gluon fields in the early stage. $\mathcal{P}_{\rm survival}$ is built similarly to the hadronization probability introduced in coalescence models [116–121]. We are able to estimate an average melting time for both $c\bar{c}$ and $b\bar{b}$ pairs, that turns out to be around 0.4–0.5 fm/c. Differently from [113], we consider $N_c = 3$ and an initialization for pA collisions that takes into account the event-by-event fluctuations of the color charges in the proton and of the initial distribution of the heavy quarks in the transverse plane. Moreover, within our model we allow for the expansion both along the longitudinal direction and in the transverse plane, while in [113] only a static geometry was considered.

Throughout this article, we use natural units $k_B = c = \hbar = 1$. Moreover, we formulate the $SU(3)$ Yang-Mills equations using the Milne coordinates

$$\tau = \sqrt{t^2 - z^2}, \qquad \eta = \frac{1}{2}\ln\left(\frac{t+z}{t-z}\right), \tag{1}$$

where τ is the proper time and η denotes the space-time rapidity.

II. THE EVOLVING GLASMA IN PROTON-NUCLEUS COLLISIONS

A. Color charges for p and A

The CGC effective theory [15–17] is based on a separation of scales between the high Bjorken-x degrees of freedom, i.e. the valence partons, and the low x degrees of freedom which they generate, that is, soft gluons. To realize this separation, the sources of the initial gluon fields are generated using the McLerran-Venugopalan (MV) model, in which the large-x color sources are randomly distributed on an infinitely thin color sheet. The distribution of these charges is a Gaussian, characterized by zero average

$$\langle \rho^a(\mathbf{x}_\perp)\rangle = 0, \tag{2}$$

and variance given by

$$\langle \rho^a(\mathbf{x}_\perp)\rho^b(\mathbf{y}_\perp)\rangle = g^2\mu^2\delta^{ab}\delta^{(2)}(\mathbf{x}_\perp - \mathbf{y}_\perp). \tag{3}$$

Here, g is the coupling constant (we use $g = 2$, corresponding to $\alpha_s = g^2/4\pi = 0.3$), and μ is the so-called MV parameter, describing the number density of the color charges per unit of area in the transverse plane. In our implementation, we relax the single-sheet hypothesis of the original MV model by generating a certain number N_s of color sheets stacked on top of one another [122]. Consequently, for each of the sheets, the numerical implementation of Eq. (3) we will use in this work is

$$\langle \rho^a_{n,x}\rho^b_{m,y}\rangle = g^2\mu^2\frac{\delta_{n,m}}{N_s}\delta^{a,b}\frac{\delta_{x,y}}{a_\perp^2}, \tag{4}$$

where $a, b = 1, \ldots, N_c^2 - 1$ are $SU(3)$ color indexes, $n, m = 1, \ldots, N_s$ are the color sheet indexes and x, y span each point of a $N_\perp \times N_\perp$ lattice, whose transverse length is $L_\perp$ and lattice spacing is $a_\perp = L_\perp/N_\perp$. Operatively, conditions (2) and (4) are satisfied by generating random Gaussian numbers with mean zero and standard deviation equal to $\sqrt{(g^2\mu^2)/(N_s a_\perp^2)}$. Below we explain, starting

from these color charges, how to build up the gluon fields generated by each sheet, and how to combine all these fields to obtain the initial gluon field in the glasma. We use $N_s = 50$ in Eq. (4), having checked that this number of sheets is enough to get numerical convergence.

These steps are shared by the charge generation of both a proton and a heavy ion. The original MV model assumed a source charge density that is homogeneous in the transverse plane. We adopt this assumption when dealing with large-A nuclei, whose details at the level of single nucleons can be neglected. On the other hand, a reasonable description of protons involves a varying nuclear density in the transverse plane to take into account the underlying quark structure. The main difference between those two cases lies in the choice of μ: in the A-case μ is chosen as a constant equal to $\mu = 0.5$ GeV, which translates into uniform fluctuations of color charge throughout the lattice. The p-case is instead more involved. In order to do so, let us introduce the thickness function of the proton T_p, normalized to 1 and defined as

$$T_p(\mathbf{x}_\perp) = \frac{1}{3}\sum_{i=1}^{3}\frac{1}{2\pi B_q}\exp\left(-\frac{(\mathbf{x}_\perp - \mathbf{x}_i)^2}{2B_q}\right), \tag{5}$$

where the $\mathbf{x}_i$ denote the positions of the constituent quarks, which are randomly extracted from the distribution

$$T_{cq}(\mathbf{x}_\perp) = \frac{1}{2\pi B_{cq}}\exp\left(-\frac{\mathbf{x}_\perp^2}{2B_{cq}}\right). \tag{6}$$

Parameters have been chosen as $B_q = 0.3$ GeV^{-2}, $B_{cq} = 4$ GeV^{-2}, i.e., the widths of the two Gaussians differ by a factor around 4. After doing so, we evaluate the saturation scale Q_s in this model as

$$Q_s^2(x, \mathbf{x}_\perp) = \frac{2\pi^2}{N_c}\alpha_s x g(x, Q_0^2) T_p(\mathbf{x}_\perp). \tag{7}$$

from which $\mu(x, \mathbf{x}_\perp)$ is given by [123]

$$g^2\mu(x, \mathbf{x}_\perp) = c Q_s(x, \mathbf{x}_\perp), \tag{8}$$

with $c = 1.25$. Note that by virtue of Eq. (7) not only μ, but also Q_s depend on the transverse plane coordinates. Also, in principle xg in (7) should be computed at the scale Q_s by means of the Dokshitzer-Gribov-Lipatov-Altarelli-Parisi (DGLAP) equation with a proper initialization. This was done in [123,124], and we reserve this approach for future studies. For the sake of simplicity, in the present study we limit ourselves by assuming that xg is given by the initial condition at $Q_0^2 = 1.51$ GeV^2 as in [123,124], namely

$$x g(x, Q_0^2) = A_g x^{-\lambda_g}(1-x)^{f_g}, \tag{9}$$

with $A_g = 2.308$, $\lambda_g = 0.058$, and $f_g = 5.6$. This simplification is partly justified by the fact that the average saturation scale for the proton is of the order of $Q_s \sim 1$ GeV, hence we do not expect the DGLAP evolution of the xg in Eq. (9) to lead to significant changes. For pA collisions at the LHC energy, the relevant values of x are in the range $[10^{-4}, 10^{-3}]$. In our calculations, we will thus fix x in the aforementioned range, then compute xg by virtue of Eq. (9). We will use the corresponding value obtained for $x = 10^{-4}$, that is, $xg = 3.94$.

B. Gauge-link formulation of the evolving glasma

Once the charge has been generated, we know that the hard and the soft sectors are coupled via the Yang-Mills equations [125]

$$D_\mu F^{\mu\nu} = J^\nu, \tag{10}$$

where $D_\mu = \partial_\mu - ig[A_\mu, \cdot]$ is the covariant derivative, $F^{\mu\nu} = \partial^\mu A^\nu - \partial^\nu A^\mu - ig[A^\mu, A^\nu]$ is the field strength tensor and J^μ the color current. Using the light-cone coordinates, the conservation of current implies $A^- = 0$. Moreover, by working in the covariant gauge we can also impose $A^i = 0$, where $i = x, y$. The only component left is therefore $A^+ \equiv \alpha$, which can be seen to obey the following Poisson equation

$$\Delta_\perp \alpha(\mathbf{x}_\perp) = -\rho(\mathbf{x}_\perp). \tag{11}$$

In order to solve this equation, we introduce a soft regulator, m, then Fourier-transform both sides of (11), getting

$$\tilde{\alpha}^a_{n,k} = \frac{\tilde{\rho}^a_{n,k}}{\tilde{k}_\perp^2 + m^2}, \tag{12}$$

where the discretized momentum $\tilde{k}_\perp$ is given by

$$\tilde{k}_\perp^2 = \sum_{i=x,y}\left(\frac{2}{a_\perp}\right)^2 \sin^2\left(\frac{k_i a_\perp}{2}\right), \tag{13}$$

and $m = 0.2$ GeV $= 1$ fm^{-1}, which acts as a screening mass and effectively implements color confinement on lengths above $1/m$. By then, Fourier-transforming back, we get $\alpha(\mathbf{x}_\perp)$ in coordinate space.

Once we obtained a solution for the gauge field in the covariant gauge, the Wilson line for each nucleus is evaluated as

$$V_{\mathbf{x}} = \prod_{n=1}^{N_s}\exp\{ig\alpha^a_{n,\mathbf{x}} T^a\} \tag{14}$$

and then obtain the gauge links, U, for each of the two nuclei as

$$U^{A,B}_{\mathbf{x},i} = V^{A,B}_{\mathbf{x}} V^{\dagger,A,B}_{\mathbf{x}+\hat{i}}. \tag{15}$$

In the above expressions, T^a are the $SU(3)$ group generators in the fundamental representation, with normalization $\mathrm{Tr}[T^a T^b] = \delta^{ab}/2$. Periodic boundary conditions have been implemented on the transverse plane.

The gauge link resulting from the interaction of the two colored glasses in p and A, $U_{\boldsymbol{x},i}$, at the position $\boldsymbol{x}$ in the transverse plane is determined by solving a set of eight equations, which are

$$\mathrm{Tr}[T_a(U^A_{\mathbf{x},i} + U^B_{\mathbf{x},i})(\mathbb{I} + U_{\mathbf{x},i}) - \mathrm{H.c.}] = 0, \tag{16}$$

with $a = 1, \ldots, N_c^2 - 1$. In the case of $N_c = 2$ there is an exact solution of (16) for $U_{\mathbf{x},i}$ [126]. Instead, for $SU(3)$ we can solve (16) only numerically via a standard iterative method. Using this procedure we calculate the gauge links along the x and y direction. For the longitudinal components we initialize simply $U_\eta = \mathbb{I}$ since the glasma has $A_\eta = 0$ at $\tau = 0^+$. The initial color-electric fields are [127]

$$\begin{aligned} E_x &= E_y = 0, \\ E^\eta &= -\frac{i}{4ga_\perp^2}\sum_{i=x,y}[(U_i(\mathbf{x}_\perp) - \mathbb{I})(U_i^{B,\dagger}(\mathbf{x}_\perp) - U_i^{A,\dagger}(\mathbf{x}_\perp)) \\ &\quad + (U_i^\dagger(\mathbf{x}_\perp - \hat{\imath}) - \mathbb{I})(U_i^{B,\dagger}(\mathbf{x}_\perp - \hat{\imath}) \\ &\quad - U_i^{A,\dagger}(\mathbf{x}_\perp - \hat{\imath})) - \mathrm{H.c.}]. \end{aligned} \tag{17}$$

After the initial condition has been fixed, The equations of motion for the gauge links are [127]

$$\partial_\tau U_i(\mathbf{x}) = \frac{-iga_\perp}{\tau} E^i(\mathbf{x}) U_i(\mathbf{x}), \tag{18}$$

$$\partial_\tau U_\eta(\mathbf{x}) = -iga_\eta \tau E^\eta(\mathbf{x}) U_\eta(\mathbf{x}), \tag{19}$$

where a_η denotes the discretization step in the η direction. In order to reduce the discretization error in time, we drive the evolution through a leapfrog algorithm, i.e. by letting the gauge links and the electric fields evolve in different steps alternatively. Equations (18) and (19) are discretized as

$$U_i(\tau'') = \exp[-2\Delta\tau iga_\perp E^i(\tau')/\tau'] U_i(\tau), \tag{20}$$

$$U_\eta(\tau'') = \exp[-2\Delta\tau iga_\eta \tau' E^\eta(\tau')] U_\eta(\tau), \tag{21}$$

where $\tau' = \tau + \Delta\tau/2$ and $\tau'' = \tau + \Delta\tau$. Notice that the exponentiation of the electric field is important, in order to keep the up-to-date gauge links as unitary matrices. In the same fashion, the equations of motion of the electric field are discretized as

$$\begin{aligned} E^i(\tau') &= E^i(\tau - \Delta\tau) + 2\Delta\tau \frac{i}{2ga_\eta^2 a_\perp \tau}[U_{\eta i}(\tau) + U_{-\eta i}(\tau) \\ &\quad - (\mathrm{H.c.})] + 2\Delta\tau \frac{i\tau}{2ga_\perp^3}\sum_{j\neq i}[U_{ji}(\tau) \\ &\quad + U_{-ji}(\tau) - (\mathrm{H.c.})], \\ E^\eta(\tau') &= E^\eta(\tau - \Delta\tau) + 2\Delta\tau \frac{i}{2ga_\eta a_\perp^2 \tau}\sum_{j=x,y}[U_{j\eta}(\tau) \\ &\quad + U_{-j\eta}(\tau) - (\mathrm{H.c.})], \end{aligned} \tag{22}$$

where

$$U_{\mu\nu}(\mathbf{x}) \equiv U_\mu(\mathbf{x}) U_\nu(\mathbf{x} + \hat{\mu}) U_\mu^\dagger(\mathbf{x} + \hat{\nu}) U_\nu^\dagger(\mathbf{x}) \tag{23}$$

are the plaquette variables. Notice that in this way the gauge links are initialized at time $\tau = 0$, and evolve with integer steps: $\tau = \Delta\tau, 2\Delta\tau, \ldots$ Instead, the electric field is initialized at $\tau = \Delta\tau/2$ and proceeds as $\tau = 3\Delta\tau/2, 5\Delta\tau/2, \ldots$ Along with the electric field, using the gauge links we can derive the components of the color-magnetic field as [127]

$$B_x^a = \frac{2}{iga_\eta \tau a_\perp}\mathrm{Tr}[T^a(\mathbb{I} - U_{\eta y})], \tag{24}$$

$$B_y^a = \frac{2}{iga_\eta \tau a_\perp}\mathrm{Tr}[T^a(\mathbb{I} - U_{\eta x})], \tag{25}$$

$$B_z^a = \frac{2}{iga_\perp^2}\mathrm{Tr}[T^a(\mathbb{I} - U_{xy})]. \tag{26}$$

III. HEAVY QUARK DYNAMICS IN THE PRE-EQUILIBRIUM STAGE

In this section, we discuss how we model the diffusion of the heavy quark pairs in the pre-equilibrium stage. Following [113], we model the dynamics of the quarks in the $c\bar{c}$ and $b\bar{b}$ pairs using semiclassical equations of motion, namely the Wong equations. They describe the time evolution of the coordinate $\mathbf{x}$, momentum $\mathbf{p}$, and color charge Q_a (with $a = 1, \ldots, N_c^2 - 1$) of the quarks [114,115]. In the laboratory frame, the Wong equations read

$$\frac{\mathrm{d}x^i}{\mathrm{d}t} = \frac{p^i}{E}, \tag{27}$$

$$\frac{\mathrm{d}p^i}{\mathrm{d}t} = gQ^a F^{i\mu,a}\frac{p_\mu}{E} - \frac{\partial V}{\partial x_i}, \tag{28}$$

$$\frac{\mathrm{d}Q_a}{\mathrm{d}t} = -gf^{abc}A_\mu^b Q_c \frac{p^\mu}{E}, \tag{29}$$

where $i = x, y, z$ and $\mu = 0, \ldots, 3$. Moreover, f^{abc} are the structure constants of the gauge group $SU(N_c)$ and $E = \sqrt{\boldsymbol{p}^2 + M^2}$ is the kinetic energy of the quark with

mass M. The Wong equations have been recently used to study the dynamics of the heavy quarks in the pre-equilibrium stage of high-energy nuclear collisions; see [67–70,74,76,83,84,113,128–130] and references therein.

The gauge field A_μ in Eq. (29) is determined by (the A_τ component is zero because of the gauge choice)

$$A_i(\mathbf{x}) = -\left(\frac{i}{g a_\perp}\right) \log U_i(\mathbf{x}), \quad i = x, y, \tag{30}$$

$$A_\eta(\mathbf{x}) = -\left(\frac{i}{g a_\eta}\right) \log U_\eta(\mathbf{x}), \tag{31}$$

whereas the color-electric and color-magnetic fields are defined in terms of the field strength tensor through

$$F_{\tau i} = E_i, \qquad F_{\eta i} = \tau \epsilon_{ij} B_j, \tag{32}$$

$$F_{\tau\eta} = \tau E_\eta, \qquad F_{xy} = -B_\eta. \tag{33}$$

For $N_c = 3$ the evolution of the color charges governed by Eq. (29) conserves the Casimir invariants

$$q_2 = Q_a Q_a, \qquad q_3 = d_{abc} Q_a Q_b Q_c, \tag{34}$$

with

$$q_2 = \frac{N_c^2 - 1}{2} \quad \text{and} \quad q_3 = \frac{(N_c^2 - 4)(N_c^2 - 1)}{4 N_c}, \tag{35}$$

and d_{abc} are the symmetric structure constants [80]. We solve Eqs. (27)–(29) in the background of the evolving glasma fields. Within our model, we follow previous works and neglect the back-reaction of the quarks in the Yang-Mills equations: it has been shown [70] that such back-reaction does not substantially affect the diffusion of heavy quarks within the lifetime of the pre-equilibrium stage.

In Eq. (28) V denotes the interaction potential between a quark and its respective antiquark in the pair. In QCD, the tree-level static potential between a quark and an antiquark can be written as

$$V_{\alpha\beta\gamma\delta} = \frac{\alpha_s}{r_{\rm rel}} T^a_{\alpha\beta} \bar{T}^a_{\gamma\delta}, \tag{36}$$

which is related to the static limit of the amplitude of the one-gluon-exchange interaction between two quarks in the color states β and δ that go out respectively in the color states α and γ. The $\bar{T}^a$ correspond to the generators in the $\bar{\mathbf{3}}$ representation. In (36) the quantity $r_{\rm rel} = |\mathbf{x}_Q - \mathbf{x}_{\bar{Q}}|$, is the relative distance between the quark and the antiquark.

This potential depends on the matrix element of the operator $T^a \otimes \bar{T}^a$, where the first color generator acts on the Hilbert space of the quark, and the second on that of the antiquark. The potential (36) can be projected onto irreducible representations of $SU(3)$. In particular, if the quark-antiquark pair belongs to the irreducible representation R we have

$$V_R = \lambda_R \frac{\alpha_s}{r_{\rm rel}}, \tag{37}$$

where

$$\lambda_R = \frac{1}{2}[C_2(R) - C_2(3) - C_2(\bar{3})]. \tag{38}$$

Here, $C_2(R)$ denotes the eigenvalue of the quadratic Casimir in the representation R, while $C_2(3) = C_2(\bar{3}) = 4/3$ are the Casimir for the quark and the antiquark in the 3 and $\bar{\mathbf{3}}$ representations respectively. If the quark-antiquark pair is in the color-singlet representation then $C_2(1) = 0$ and

$$V_1 = -\frac{4}{3}\frac{\alpha_s}{r_{\rm rel}}. \tag{39}$$

Similarly, for the octet $C_2(8) = 3$ and

$$V_8 = +\frac{1}{6}\frac{\alpha_s}{r_{\rm rel}}. \tag{40}$$

Within our semiclassical approach, the most natural choice for V in Eq. (28) consists in replacing $T^a \otimes T^a$ in Eq. (36) with $Q_a \bar{Q}_a / N_c$. Hence, in Eq. (28) we consider

$$V = \frac{Q_a \bar{Q}_a}{N_c} \frac{\alpha_s}{r_{\rm rel}}. \tag{41}$$

The overall $1/N_c$ in the right hand side of (41) is included in order to reproduce $V = V_1$ when we initialize the pairs in a color-singlet state, see below Eq. (50). For each pair, $Q_a \bar{Q}_a$ evolves with time, therefore the coupling in V follows the evolution of the color charges as a result of the interaction with the background gluon fields. For a justification of Eq. (41) starting from the expectation value of the QCD potential see Sec. V B.

Before going ahead, we notice that in [113] a similar problem was studied, although for the simpler geometry of a static box and for the $SU(2)$ gauge group. The improvement that the potential (41) brings with respect to the one used in [113], namely a pure singlet potential, is that our V dynamically evolves with the color charges of the pair, so it takes into account that even if the pairs are initialized in color-singlet states, they can get an octet component due to the interaction with the background gluon fields.

IV. HEAVY QUARKS INITIALIZATION

Both $c\bar{c}$ and $b\bar{b}$ quark pairs are produced by hard QCD scatterings among the nucleons of the colliding nuclei at the very early stage of high-energy nuclear collisions, within

0.1 fm/c from the overlap of the two initial nuclei. In this work, we assume the pairs to form at proper time $\tau_{\rm form} = 1/(2M)$, with M being the heavy-quark mass: $M = 1.3$ GeV for c and $M = 4.2$ GeV for b. Therefore $\tau_{\rm form} \sim 0.08$ fm/c for c, and $\tau_{\rm form} \sim 0.02$ fm/c for b.

A. Initialization in the coordinate space and in momentum space

In this work we consider the pairs produced at mid-rapidity, so that the longitudinal coordinate of the heavy quarks is kept $z = 0$, if we indicate with positive z and negative z respectively the forward-going and backward-going directions of the colliding nuclei. In the transverse plane, the initial positions of the heavy quarks are extracted on an event-by-event basis. For each event, after extracting the position of the three valence quarks via the Gaussian profile (6), we extract the position of the center of mass of each quark-antiquark pair via the profile (5). In this way, the heavy quarks are distributed around the hot spots of the initial energy density of the color fields. From that, we extract the relative distance between each quark and antiquark in the pair (in its rest frame) according to the distribution

$$P_{\rm HQ}(r_{\rm rel}) = r_{\rm rel} \exp\left(-r_{\rm rel}^2/r_0^2\right), \tag{42}$$

where $r_0 = 0.4$ fm for a $c\bar{c}$ pair and $r_0 = 0.2$ fm for a $b\bar{b}$ [131]. Using the $r_{\rm rel}$ we extract for each pair, each quark is placed at a distance $r_{\rm rel}/2$ from the center of mass of the pair, while the polar angle is extracted uniformly in the range $(0, 2\pi)$. The corresponding antiquark is generated opposite to the quark, with respect to the center of mass. For illustrative purposes, we show in Fig. 1 the centers of mass of 100 heavy-quark pairs in two events. We remark that this number of pairs is chosen only for a good visualization and does not correspond to the real number of quarks produced in the considered collision system. In both panels of the figure, the three hot spots correspond to the profile (5) that develops around the three valence quarks, whose location changes event-by-event; we checked that these are the same locations where most of the energy density gets deposited at the initial time. The red dots represent the centers of mass of the production points of the heavy quark and antiquark in the pairs.

Moving on to the initialization in momentum space, we extract the modulus of the relative momentum in transverse plane of each quark and antiquark in the pair (in its rest frame) according to the distribution

$$P_{\rm HQ}(p_{\rm rel}) = p_{\rm rel} \exp\left(-p_{\rm rel}^2 r_0^2\right), \tag{43}$$

Once $p_{\rm rel}$ is extracted for each pair, we set the modulus of the quark momentum as $p_{\rm rel}/2$, while the polar angle is extracted uniformly in the range $(0, 2\pi)$. From that, the components p_x and p_y of the heavy-quark momentum are determined and those of the companion antiquark are fixed opposite to them. We assume $p_z = 0$ for quarks and their companion antiquarks, as we simulate the mid-rapidity region and assume that the space-time rapidity of the produced particles η is equal to the energy-momentum rapidity y. With this initialization of momenta the quark and antiquark in a pair have momenta, $\boldsymbol{p}_q$ and $\boldsymbol{p}_{\bar{q}}$ respectively, such that the total momentum is zero, $\boldsymbol{p}_q + \boldsymbol{p}_{\bar{q}} = 0$. Note also that the width of the gaussian (43) is set as $1/r_0$, being r_0 the same parameter used in (42) for the initialization in coordinate space. The HQs in a $b\bar{b}$ pair will therefore be initialized with an average momentum which is larger than the HQs in a $c\bar{c}$ pair.

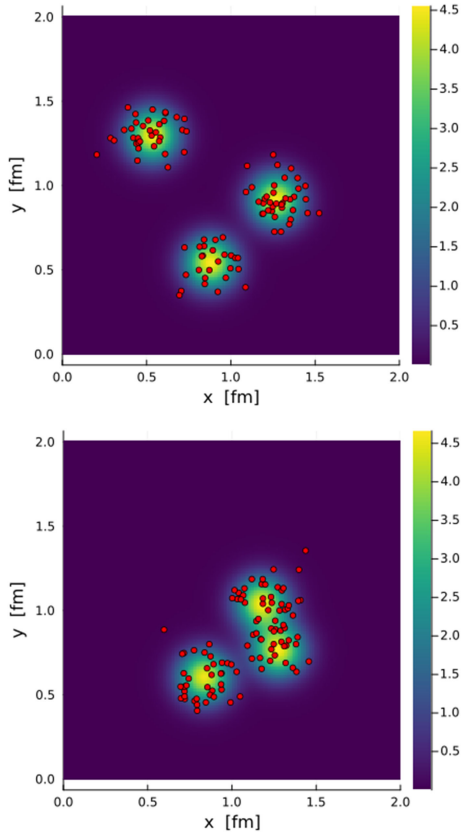

FIG. 1. Centers of mass of the production points of heavy-quark pairs (red dots) on the transverse plane for proton-nucleus collisions. The background image corresponds to the contour plot of the profile (5) in fm^{-2}, characterized by three hot spots that develop around the valence quarks in that event. We used $g\mu = 1$ GeV for the nucleus. The two panels correspond to two different events.

B. Initialization in the color space

Let us deal with the initialization of the color charges appearing in the Wong equations (28) and (29). The initial value of the color charges needs to satisfy the constraints (34). In order to get these, we first fix the charge of one

heavy quark in the ensemble to be [80]

$$Q_{0a} = -1.69469\delta_{a5} - 1.06209\delta_{a8} \tag{44}$$

which explicitly satisfies the conditions (34); then, we generate the charges of all the other heavy quarks as

$$Q_a = Q_{0b}U^{ab}, \qquad U^{ab} = 2\mathrm{Tr}[T^a U T^b U^\dagger], \tag{45}$$

where U is an $SU(3)$ random matrix which is extracted for each heavy quark according to the Haar measure. By construction, all the HQs hereby obtained satisfy (34), and this condition will be satisfied throughout the time evolution, as already stated.

As anticipated in Sec. III, we initialize the $c\bar{c}$ and $b\bar{b}$ pairs as an ensemble of color-singlet states. In a quantum-mechanical framework, this would amount to initialize the color part of the wave function of each pair as

$$|S\rangle = \frac{1}{\sqrt{3}}(|r\bar{r}\rangle + |g\bar{g}\rangle + |b\bar{b}\rangle). \tag{46}$$

For the state (46) we have

$$\langle S|\sum_a (T_1^a + \bar{T}_2^a)^2|S\rangle = 0, \tag{47}$$

where $T_{1,2}^a$ denotes the $SU(3)$ color generators acting on the Hilbert spaces of the quark and the antiquark respectively. In the classical limit, we replace operators with their expectation values. Denoting by Q_a and $\bar{Q}_a$ the color charges of, respectively, the quark and the antiquark in a pair, the classical version of Eq. (47) reads

$$\sum_a (Q_a + \bar{Q}_a)^2 = 0, \tag{48}$$

which immediately implies

$$Q_a = -\bar{Q}_a, \quad a = 1, \ldots, \qquad N_c^2 - 1. \tag{49}$$

This also implies that, by taking into account the normalization of the classical charges (34), at initial time we have

$$\sum_a Q_a \bar{Q}_a = -q_2. \tag{50}$$

Hence, we initialize the color charge of each antiquark by imposing the condition (49).

V. RESULTS

In this section, we show our results on the heavy-quark evolution and heavy quark-antiquark pair dissociation in proton-nucleus collisions at LHC energy. The results shown in this section have been obtained for a square grid of transverse size $L = 3$ fm, with 64×64 lattice points. In realistic collisions, the pre-equilibrium stage lasts for a fraction of fm/c, but for illustrative purposes we performed simulations up to 1 fm/c with 1000 time steps (we checked that this number of time steps is enough to have numerical convergence).

In each simulation we considered 1000 HQ pairs, for a total of 2000 particles. We remark that the pairs used in our simulation serve as test particles and their number does not correspond to the number of actual pairs produced in the collisions. Since we will only focus on percentages and fractions over the total number of pairs, such value is chosen purely for statistical reasons.

We consider all the pairs to be independent on each others. This is motivated by the net average number of formed pairs in a pA collision, which is very small. This can be estimated as follows. For Pb-Pb collisions in the 0–10% centrality class, it has been estimated that $\langle N_{c\bar{c}\mathrm{pairs}}\rangle \approx 15$ (see for example [132]). From this, we can extrapolate the average number of pairs in p-Pb collisions by scaling $\langle N_{c\bar{c}\mathrm{pairs}}\rangle$ with the number of binary collisions, N_{coll}. The latter can be computed by the average μ^2 of the proton and the nucleus, being $\mu^2 \propto T$ where T denotes the thickness function. In particular, within our implementation, for the nucleus we have $\langle\mu^2\rangle_A = (0.5\ \mathrm{GeV})^2$, it being trivially constant in the interaction region. For the proton, we use Eqs. (7) and (8) to get $\mu(\mathbf{x}_\perp)$, then we integrate over all constituent quark configurations and over the transverse plane, and finally divide by the area of the proton. We get

$$\langle\mu^2\rangle_p = \frac{\int \mathrm{d}^2\mathbf{x}_i \int \mathrm{d}^2\mathbf{x}_\perp \mu^2 T_{cq}(\mathbf{x}_\perp)}{\pi R_p^2} = \frac{c^2 x g}{6 g^2 R_p^2}, \tag{51}$$

where we put $R_p = 1$ fm for the radius of the proton, and $T_{cq}(\mathbf{x}_\perp)$ given by (6). Consequently,

$$\frac{N_{\mathrm{coll}}^{pA}}{N_{\mathrm{coll}}^{AA}} = \frac{\langle\mu^2\rangle_p \langle\mu^2\rangle_A}{\langle\mu^2\rangle_A^2} \approx \frac{1}{25}. \tag{52}$$

This gives $\langle N_{c\bar{c}\mathrm{pairs}}\rangle \approx 0.6$ in p-Pb. For $b\bar{b}$ the numbers are even smaller: one can estimate a cross section for $b\bar{b}$ production which is 25 smaller with respect to $c\bar{c}$ production [133,134]. Therefore the system of $c\bar{c}$ and $b\bar{b}$ pairs is very dilute and interaction among different pairs is negligible, which justifies our assumption of independent pairs.

In our numerical implementation, following [113] we cure the numerical divergence for $r_{\mathrm{rel}} = 0$ in (41) by using in Eq. (28) the regularized potential

$$V = \frac{Q_a \bar{Q}_a}{N_c} \frac{\alpha_s}{r_{\mathrm{rel}}}(1 - e^{-A r_{\mathrm{rel}}}), \tag{53}$$

instead of (41). Here we present results obtained with $A = (0.017\ \mathrm{fm})^{-1}$: we checked that taking A larger than

this value makes the screening of the divergence at $r_{\rm rel} = 0$ ineffective, not leading to the convergence of the numerical algorithm.

A. Spreading and color decorrelation of the pairs

Let us focus on heavy quark-antiquark pairs and investigate the effect of the evolving glasma in dissociating the initially produced pairs. The relative position of the quark and antiquark in the pairs is modified during their propagation in the fireball, both in the pre-equilibrium and in the thermalized QGP phases. In particular, the interaction with the gluon fields leads to a diffusion in coordinate (as well as momentum) space, resulting on average in the increase of the relative distance of the two particles in a pair.

In Fig. 2 we plot the relative distance of c and $\bar{c}$ in $c\bar{c}$ pairs, $r_{\rm rel}$, in the rest frame of the pairs, versus the proper time τ (measured with respect to the formation time $\tau_{\rm form}$), averaged over the HQ pairs as well as over the gauge field configurations. We show our results in four different cases: along with the result obtained with the dynamic potential (41) (solid green), we plot $r_{\rm rel}$ obtained by considering $V = 0$ in Eq. (28) (solid red), by using $V = V_1$ defined in Eq. (39) (solid blue), as well as by turning off the gluon fields (solid black). The latter is shown in order to illustrate the quantitative effect of the HQ potential and of the gluon fields on $r_{\rm rel}$.

In the scenario in which only the potential is considered, $r_{\rm rel}$ decreases over time due to the attractive interaction between the quark and the antiquark in the pair. Indeed, in this case the dynamical potential coincides with the singlet potential, since the color charges do not evolve under the action of the glasma. On the other hand, we see that the effect of the glasma is to increase the separation of the pair, due to the intense bombardment of gluons on both the quark and antiquark of the pair. Notably, during the time interval where the glasma framework is phenomenologically relevant, i.e., up to approximately 0.3–0.4 fm/c, $r_{\rm rel}$ remains nearly constant. This behavior results from the competition between the attractive potential and the interaction with the color fields of the glasma.

For completeness, in Fig. 2 we also display the case where the potential is absent. By comparing this with the full calculation, we observe that, as expected, the presence of an attractive potential leads to an initial decrease in $r_{\rm rel}$. Finally, when the potential is modeled as a pure singlet interaction, $r_{\rm rel}$ remains very close to the result of the full calculation within the time range where the glasma is phenomenologically relevant. This suggests that, during this period, the interaction between the quarks in the pair is not significantly different from that of a pure singlet. On the other hand, moving on at later times, $r_{\rm rel}$ in the pure singlet scenario is slightly lower if compared to the full calculation. This is a natural consequence of the fact that the singlet potential remains stronger than the full potential

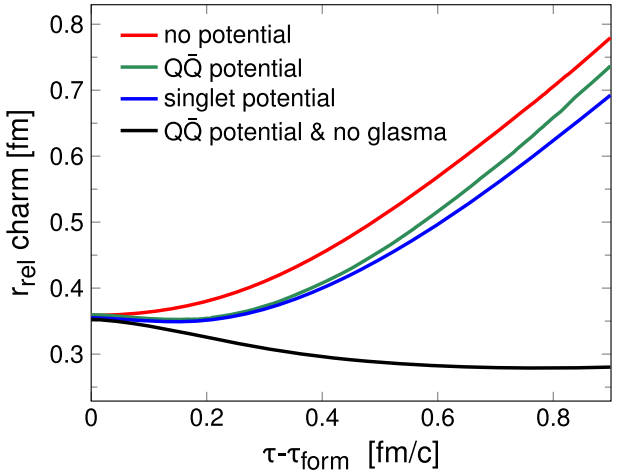

FIG. 2. Averaged relative distance for $c\bar{c}$ pairs, computed in the pair rest frame. The no potential data correspond to calculations without the potential (41) in the Wong equation (28). $Q\bar{Q}$ potential denote the results obtained considering the potential as well as the evolving glasma fields. Blue line stands for the results obtained assuming a pure color-singlet potential in Eq. (28). Finally, the $Q\bar{Q}$ potential and no glasma curve denotes the results obtained by solving the equations of motion switching off the interaction of the quarks with the fields.

at larger times, leading to a tighter binding of the quark-antiquark pairs.

By now limiting ourselves to the physical case of the potential in Eq. (41), in the top panel of Fig. 3 we show $r_{\rm rel}$ in the pair rest frame versus $\tau - \tau_{\rm form}$ for a $c\bar{c}$ pair (same solid green curve of Fig. 2) and for a $b\bar{b}$ pair (solid brown). Even when taking into account the different initialization in position for charm and beauty, we interestingly note that the $c\bar{c}$ system spreads slightly more quickly with respect to the $b\bar{b}$ one. This is expected since the higher masses of b make them more static in the gluon fields.

Not only coordinates and momenta of heavy quarks are affected by the background gluon fields, but also their color charges are, see Eq. (29). The quark-antiquark pairs can undergo transitions from singlet to octet (and vice versa) both in glasma and in QGP. In the latter stage, such transitions have been studied especially within the framework of open quantum systems [90,93,98]. These singlet-octet transitions may also occur in the glasma stage due to the interaction of the quark and antiquark in the pair with the initial color fields. For this reason we study the decorrelation of the color charges of the quark and the antiquark in a pair, which serves as an estimate of the probability of singlet-to-octet transitions, and hence gives indications on the survival probability of the pair in the gluon fields.

As explained in Sec. IV B, we initialize the quark-antiquark pairs in color-singlet states, then the interactions with the gluonic environment changes their color charges. Denoting by Q_a and $\bar{Q}_a$ the color charges of a quark and its

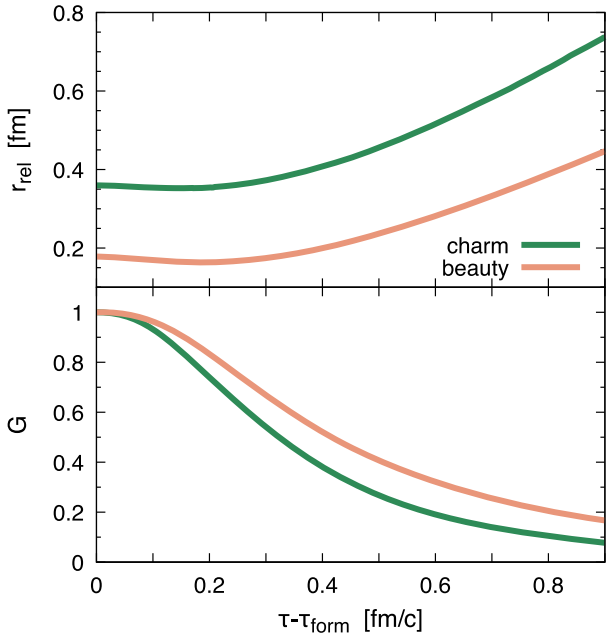

FIG. 3. Averaged relative coordinate in the pair rest frame (top panel) and color-charge correlator (bottom panel) of the heavy quark-antiquark pairs versus time $\tau - \tau_{\rm form}$, with $\tau_{\rm form}$ being the heavy-quark formation time. Green and brown curves correspond to charm and beauty heavy-quark pairs, respectively.

antiquark respectively, let us consider for each pair the time-dependent quantity

$$\mathcal{G}(\tau) = -\frac{1}{q_2}\mathrm{Tr}(Q_a(\tau)\bar{Q}_b(\tau)) = -\frac{1}{q_2}\sum_a Q_a(\tau)\bar{Q}_a(\tau), \quad (54)$$

where q_2 is the quadratic Casimir invariant of $SU(N_c)$ introduced in (35), and the trace is understood over the (a, b) indices. For the color-singlet initialization we have $Q_a = -\bar{Q}_a$ at $\tau = \tau_{\rm form}$, therefore for each pair

$$\mathcal{G} = 1 \quad \text{at } \tau = \tau_{\rm form}, \quad (55)$$

indicating that with our initialization the color charges of the two particles at $\tau = \tau_{\rm form}$ are maximally anticorrelated. We expect that on average the magnitude of $\mathcal{G}$ decreases with time, as a result of the decorrelation of Q_a and $\bar{Q}_b$ due to the random interactions with the gluon fields of the evolving glasma. This decrease can be interpreted as the raising of the weight of the color-octet component in the pair, which eventually leads to the melting of the pair itself. We will use this idea to define a melting probability of the $c\bar{c}$ and $b\bar{b}$ pairs, see Sec. V C.

From the above definition (54) of $\mathcal{G}$, we define the gauge-invariant color-charge correlator as [113]

$$G(\tau) \equiv \langle \mathcal{G}(\tau) \rangle. \quad (56)$$

The brackets in (56) indicate the average over the pairs as well as over the gauge field configurations. In the lower panel of Fig. 3 we plot $G(\tau)$ versus time $\tau - \tau_{\rm form}$, for charm (green line) and beauty (brown line) pairs. We notice that G decreases with time, as expected, indicating a decorrelation of the color charges of the quark and of the companion antiquark in the pair.

In order to be more quantitative we define a decorrelation time, $\tau_{\rm dec}$, via the requirement that $G(\tau_{\rm dec}) = 1/2$. We notice that $\tau_{\rm dec} - \tau_{\rm form}$ stays in the range (0.3, 0.4) fm/c for both charm and beauty. We also find that $\tau_{\rm dec} - \tau_{\rm form}$ for b quarks is larger than the corresponding quantity computed for the c quarks: this is most likely due to the fact that $b\bar{b}$ pairs are tighter, hence they spend more time within a single correlation domain of the gluonic background.

We could interpret $G(\tau)$ as the probability for pairs to stay in the singlet channel during propagation in the pre-equilibrium stage, or equivalently, $1 - G(\tau)$ is the probability to have singlet-to-octet fluctuations. In fact, during the evolution, the decrease of the correlator can be interpreted as the fluctuations of the color charges becoming increasingly more important, making transitions to a color-octet state more probable.

One of the interesting aspects shown in Figs. 2 and 3 is that, while the interquark relative distance within the pairs remains nearly constant up to $\tau \approx 0.3$ fm/c for both c and b quark pairs, color decorrelation occurs rather quickly. In this time range, it is therefore color decorrelation that primarily drives the melting of the pair.

B. Color equilibration

The results shown in the lower panel of Fig. 3 can be rephrased in terms of the expectation values of the color-projector operators, that allow us to measure the probability of pairs to be in the color-singlet and the color-octet states. To this end, we recall that in QCD one can introduce the projectors onto the singlet, $\mathcal{P}_S$, and the octet, $\mathcal{P}_O$, spaces as

$$\mathcal{P}_S = -\frac{2}{3}T^a \otimes \bar{T}^a + \frac{1}{9}I, \quad (57)$$

$$\mathcal{P}_O = \frac{2}{3}T^a \otimes \bar{T}^a + \frac{8}{9}I, \quad (58)$$

which can be easily obtained from the eigenvalues of the operator $T^a \otimes \bar{T}^a$ in the color-singlet, λ_S, and color-octet, λ_O, representations, namely

$$\lambda_S = -\frac{4}{3}, \qquad \lambda_O = +\frac{1}{6}. \quad (59)$$

It is easy to verify that $\mathcal{P}_S^2 = \mathcal{P}_S$, $\mathcal{P}_O^2 = \mathcal{P}_O$, $\mathcal{P}_O\mathcal{P}_S = \mathcal{P}_S\mathcal{P}_O = 0$, and $\mathcal{P}_O + \mathcal{P}_S = 1$. The classical counterpart of the projectors (57) and (58) can be written as

$$P_S = -\frac{2}{3}\frac{Q_a\bar{Q}_a}{N_c} + \frac{1}{9}, \tag{60}$$

$$P_O = \frac{2}{3}\frac{Q_a\bar{Q}_a}{N_c} + \frac{8}{9}, \tag{61}$$

which can be obtained from Eqs. (57) and (58) via the formal replacement $T^a \otimes \bar{T}^a \to Q_a\bar{Q}_a/N_c$, similarly to what we have done in writing the classical counterpart of the potential (36) in Eq. (41). It is easy to check that the singlet condition (50) implies $P_S = 1$ and $P_O = 0$.

We now want to relate P_S to the probability that the quark-antiquark pair is in the color-singlet state. In fact, in the quantum theory, the probability that the state $|\psi\rangle$ is a color-singlet is

$$p_S = |\langle\psi|\mathcal{P}_S|\psi\rangle|^2. \tag{62}$$

If $|\psi\rangle$ represents a semiclassical state, we can neglect the quantum fluctuations and we can write

$$p_S = \langle\psi|\mathcal{P}_S^2|\psi\rangle, \tag{63}$$

and taking into account that $\mathcal{P}_S^2 = \mathcal{P}_S$, we get

$$p_S = \langle\psi|\mathcal{P}_S|\psi\rangle = P_S, \tag{64}$$

where the last equality stands in the classical limit. Hence, we can interpret P_S as the probability that the semiclassical quark-antiquark state is in the color-singlet state; similarly, $P_O = 1 - P_S$ gives the probability that the pair is in the color-octet state.

The identification of P_S and P_O as the probabilities for the state to be in the singlet and octet representations, respectively, allows us to justify *a posteriori* the potential (41), as it coincides with the classical limit of the QCD potential. In fact, let us consider a linear combination of singlet, $|S\rangle$, and octet $|O_i\rangle$ with $i = 1, \ldots, 8$, states, namely

$$|\psi\rangle = c_S|S\rangle + \sum_{i=1}^{8} c_i|O_i\rangle, \tag{65}$$

with $|c_S|^2 + \sum |c_i|^2 = 1$. The QCD potential is $V = V_1\mathbf{1}_S + V_8\mathbf{1}_O$, where $\mathbf{1}_S$ and $\mathbf{1}_O$ are identities in the singlet and the octet representations, and the potentials are given by Eqs. (39) and (40). Hence, the projection of V on the state $|\psi\rangle$ is

$$\langle\psi|V|\psi\rangle = |c_S|^2V_1 + (1 - |c_S|^2)V_8. \tag{66}$$

Within our semiclassical approach, we replace $|c_S|^2$ with P_S in the right hand side of Eq. (66), see Eq. (64), and the state $|\psi\rangle$ with a classical state representing our quark-antiquark pairs. We then obtain

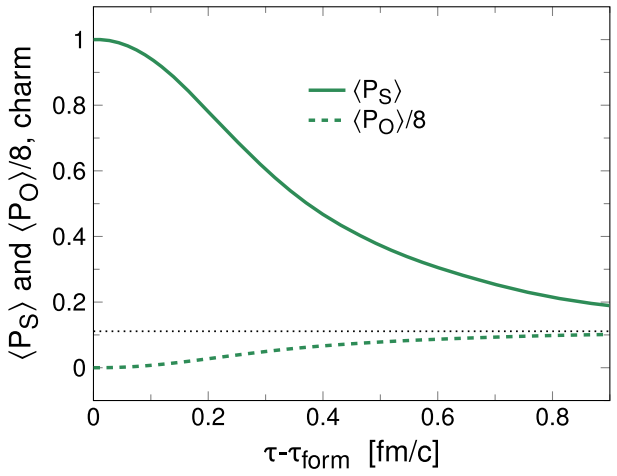

FIG. 4. Expectation values of the singlet and the (normalized) octet projectors versus proper time for $c\bar{c}$ pairs. The dashed horizontal black line stands for $1/9$. The results show the almost-perfect equipartition of probability among color-singlet and color-octet states at large times.

$$V = P_SV_1 + (1 - P_S)V_8. \tag{67}$$

Taking into account Eqs. (39), (40), and (60), we finally get Eq. (41). Therefore, we can identify the potential (41) with the classical limit of the QCD potential (66).

In Fig. 4 we plot $\langle P_S\rangle$ and $\langle P_O\rangle/8$ versus proper time, computed for $c\bar{c}$ pairs (the results for $b\bar{b}$ pairs are similar). The dashed horizontal black line stands for the value $1/9$. In particular, we divided $\langle P_O\rangle$ by eight in order to count the probability of being in one of the eight states of the octet. The results shown in the figure have been obtained by taking the ensemble average of Eqs. (60) and (61), similarly to the procedure we followed to produce the results for $G(\tau)$ shown in Fig. 3.

We notice in Fig. 4 that at the formation time the pairs are in the singlet state with probability 1, due to our initialization of the color charges. As the pairs evolve and interact with the gluon fields, there are transitions from the singlet to the octet states as a result of color decorrelation. At large times, when the colors of the quark and the antiquark in the pair are uncorrelated, the averaged projectors tend to the same value,

$$\langle P_S\rangle \approx \langle P_O\rangle/8 \approx 1/9. \tag{68}$$

This shows that asymptotically there is an equipartition of probability for the pairs to be in the singlet and in one of the eight octet states.

It is very interesting to notice that, from the qualitative point of view, the color equilibration shown in Fig. 4 is in agreement with the results of Ref. [105], in which the singlet-to-octet transitions have been studied for quarkonia states in a thermalized QGP within the framework of the quantum Brownian motion. In that context, color

equilibration takes place on a longer timescale, likely because of the different energy scales which are relevant in the two problems. Nevertheless, the interaction with the external environment (the QGP in [105] and the background gluon fields in the present work) in both cases leads to the equipartition between singlet and octet states.

We finally comment that the equilibration of color shown in Fig. 4 does not immediately lead to the statement that $1/9$ of the pairs forms a bound state at large times. In fact, in order to state anything about pair dissociation, the information on color equilibration has to be supplemented with that on the relative distance between the quark and the antiquark in the pair: on average this distance increases with time (see the upper panel in Fig. 3), therefore the pairs inevitably melt at large times even if statistically the have probability $1/9$ to be in a color-singlet state. We analyze in more detail this problem in the next subsection.

C. Melting of the pairs

We make use of the results discussed in Sec. V A to define a survival probability of the pairs in the pre-equilibrium stage, $\mathcal{P}_{\rm survival}$, and from this a melting probability

$$\mathcal{P}_{\rm melting} = 1 - \mathcal{P}_{\rm survival}. \tag{69}$$

In order to define $\mathcal{P}_{\rm survival}$, we notice in Fig. 3 that the relative distance is almost constant during the early evolution of the system, while the color of the quarks in the pairs decorrelates quickly. Therefore, it is reasonable to assume that color rotation is the leading mechanism to dissolve the pairs, hence $\mathcal{P}_{\rm survival}$ can be connected to the color-charge correlator $\mathcal{G}$ defined in Eq. (54). We assume a Gaussian shape of $\mathcal{P}_{\rm survival}$ in color space, namely

$$\mathcal{P}_{\rm survival} = \exp\left[-\kappa(\mathcal{G}-1)^2\right], \tag{70}$$

where κ is a parameter that measures the width of the fluctuations of the color charges that are necessary to break the pair. The form (70) of $\mathcal{P}_{\rm survival}$ is inspired by the Wigner function of coalescence models to form a vector meson from a quark and an antiquark of the same flavor [120]. In our model, at each time, the status of melted for each quark-antiquark pair is assigned with the probability given by Eq. (69).

We have investigated the effect of the pre-equilibrium stage on pair dissociation for several values of κ. Here, for both charm and beauty we show results for $\kappa = 4$, that corresponds to require that we have $\mathcal{P}_{\rm survival} = 1/e$ when $\mathcal{G} = 1/2$.

We quantify the impact of the early stage on the melting of the pairs by calculating the number of dissociated pairs with respect to their initial value. We show this quantity, in percentage, as a function of time $\tau - \tau_{\rm form}$ in Fig. 5 for both $c\bar{c}$ and $b\bar{b}$ pairs. By introducing the time to break half of the initial pairs, $\tau_{\rm break}$, we find $\tau_{\rm break} - \tau_{\rm form} = 0.37$ fm/c for $c\bar{c}$ pairs, and $\tau_{\rm break} - \tau_{\rm form} = 0.42$ fm/c for $b\bar{b}$ pairs. Similarly, taking $\kappa = 9/4$ that amounts to require that $\mathcal{P}_{\rm survival} = 1/e$ for $\mathcal{G} = 1/3$, we find $\tau_{\rm break} - \tau_{\rm form} = 0.43$ fm/c for $c\bar{c}$ pairs, and $\tau_{\rm break} - \tau_{\rm form} = 0.54$ fm/c for $b\bar{b}$ pairs.

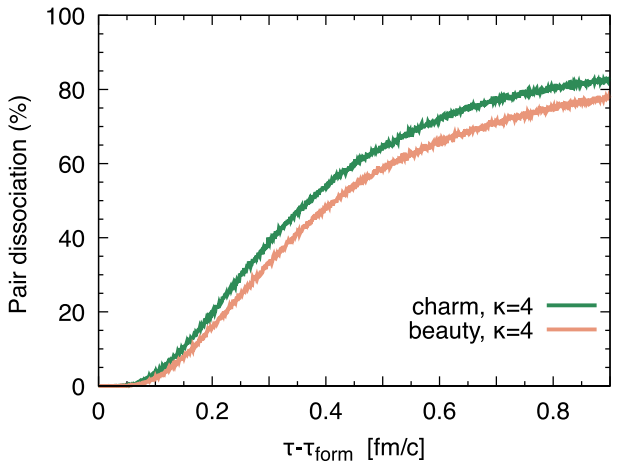

FIG. 5. Percentage of dissociated charm and bottom quark-antiquark pairs versus time $\tau - \tau_{\rm form}$, with $\tau_{\rm form}$ being the heavy quark formation time. The various curves correspond to different values of the dissociation parameters.

We conclude that the effect of the interaction of the heavy quarks with the gluon fields in the pre-equilibrium stage is to gradually melt the pairs due to the color rotation of the quark and its companion antiquark, and the time needed to break half of the initial pairs can be as small as 0.4–0.5 fm/c from the formation time. We finally notice that our results on the dissociation percentage and timescales are in the same ballpark as those shown in [113], in which the melting of pairs in the early stage was studied within a simpler model.

VI. CONCLUSIONS

We studied the melting of $c\bar{c}$ and $b\bar{b}$ pairs in the pre-equilibrium stage of high-energy proton-nucleus collisions. We modeled the early stage according to the color-glass-condensate picture, choosing the glasma as the initial condition and solving the classical Yang-Mills equations to study its evolution. The heavy quarks constituting the $c\bar{c}$ and $b\bar{b}$ pairs, which we assume to be produced in color-singlet states, are then evolved on top of the classical gluon fields via semiclassical equations of motion, known as the Wong equations. Our main goal was the calculation of the percentage of pairs that melt during their diffusion in the early stage.

We studied the evolution of the gauge-invariant correlator of the color charges of the quark and its companion antiquark, $G(\tau)$. At $\tau = \tau_{\rm form}$ we have $G(\tau_{\rm form}) = 1$ due to the color-singlet initialization of the pairs. The interaction of the quarks with the dense gluon environment leads to a degradation of the correlations. Consequently, there are

fluctuations to the color-octet state at later times, and this process favors the melting of the pairs. The timescale of decorrelation, $\tau_{\rm dec}$, can be estimated, for example, by the requirement that $G(\tau_{\rm dec}) = 1/2$. We found that $\tau_{\rm dec} - \tau_{\rm form}$ stays in the range (0.3, 0.4) fm/c for both charm and beauty. We also find that $\tau_{\rm dec} - \tau_{\rm form}$ for b quarks is larger than the similar quantity computed for the c quarks: this is most likely due to the fact that b quarks are slower, so they spend more time within correlation domains of the gluonic background.

We reformulated the decorrelation of color charges in HQ pairs in terms of color-singlet and color-octet projectors, P_S and P_O, which appear in our scheme as the classical counterparts of the quantum projection operators onto the singlet and octet representations of $SU(3)$. We identified P_S and P_O with the probabilities that the pair is in the singlet and octet states, respectively, thereby quantifying the singlet and octet components of the pair. Our findings indicate that the loss of color correlation leads to equilibration of color at large times, similarly to the results of Ref. [105] for the QGP. Specifically, we found that at large times, $\langle P_S \rangle \approx \langle P_O \rangle / 8 \approx 1/9$, which we interpret as the pair having equal probability of being in the singlet state or in one of the eight possible octet states.

The diffusion of the heavy quarks in the evolving glasma fields leads to the gradual melting of the pairs. Within our framework, the survival probability of each pair depends on the fluctuations of the color charges that generate a color-octet component for the pair and eventually break the pair itself. These are related to the gauge field fluctuations in the dense gluonic bath formed in the early stage. Within our work, we support the idea that even when the separation in coordinate space of the quarks is small, one can refer to a pair as "separated" if color-decorrelation is sufficiently large. In particular, in the early stage we find that the spatial separation is almost constant (see Fig. 2), therefore we find more effective to define a separation in the color space rather than in the coordinate space.

For each pair at a given time, we accept its survival with the probability $\mathcal{P}_{\rm survival}$ defined in Eq. (70). This probability depends on the color charges of the two particles that form the pair: these quantities are directly obtained from the solution of the Wong equations. $\mathcal{P}_{\rm survival}$ depends on one parameter, κ, that measures how large the color fluctuations need to be in order to melt the pair. We introduced a breaking time, $\tau_{\rm break}$, defined as the value of the proper time at which half of the pairs are melted. The choice of not including the relative distance in the survival probability is motivated by noticing that $r_{\rm rel}$ remains almost constant during the whole pre-equilibrium stage, as a combined effect of the attractive potential and the broadening due to the gluons in the bath. Therefore, it is natural to relate the melting probability solely to the color fluctuations. We found that for both $c\bar{c}$ and $b\bar{b}$ pairs, $\tau_{\rm break} - \tau_{\rm form}$ is approximately in the range (0.4, 0.5) fm/c Within the pre-equilibrium stage, it is color decorrelation that primarily drives the melting of the pair.

This work represents many improvements in comparison to Ref. [113], going beyond the $SU(2)$ glasma in a static box, and more importantly, including for the first time a detailed study of the color fluctuations in the pairs. Another improvement is the quark-antiquark potential for the pair, with coupling proportional to $Q_a \bar{Q}_a$, that evolves dynamically as a result of the interaction of the pair with the background gluon field. This potential accounts for the fact that the pair does not remain in a pure singlet state during the evolution, allowing for the development of an octet component due to interactions with the background gluon field. Finally, we implemented the gauge-invariant formulation in terms of gauge links and plaquettes, while in [113] the authors used the continuum formulation to solve the Yang-Mills equations.

The work presented here can be continued along several directions. First, it is desirable to link the final stage of our pre-equilibrium evolution to relativistic transport, in order to analyze the dynamics in the quark-gluon plasma stage. It is also possible to adopt a different approach, based on a master equation for the density matrix of the pairs, to analyze the color decorrelation and the melting of the pairs within a quantum-mechanical approach. Moreover, it will be interesting to analyze the same problem within different scenarios in which boost invariance is broken by longitudinal fluctuations of the background gluon field. Finally, in future developments also the interactions among all the quarks in the system, and not only within the quarks in each pair, may be taken into account. All these projects are currently under investigation and we plan to report on them soon.

ACKNOWLEDGMENTS

The authors acknowledge discussions with Dana Avramescu, Vincenzo Minissale, and Raju Venugopalan. Moreover, they acknowledge Pol Gossiaux, who suggested that they expand the discussion on color projectors and color equilibration. M. R. acknowledges Bruno Barbieri, Lautaro Martinez and John Petrucci for inspiration. L. O. acknowledges funding from the European Union—Next Generation EU, Mission 4, Component 1, CUP E63C22002960006, for the project "Heavy flavour dynamics in the early stage of ultrarelativistic collisions" (HEFESTUS). This work has been partly funded by PIACERI "Linea di intervento 1" (M@uRHIC) of the University of Catania, and the European Union—Next Generation EU through the research Grants No. P2022Z4P4B "SOPHYA—Sustainable Optimised PHYsics Algorithms: fundamental physics to build an advanced society" and No. 2022SM5YAS "Advanced probes of the Quark Gluon Plasma," under the program PRIN 2022 PNRR of the Italian Ministero dell'Università e Ricerca (MUR).

DATA AVAILABILITY

The data that support the findings of this article are openly available in [135].

[1] U. W. Heinz and M. Jacob, Evidence for a new state of matter: An assessment of the results from the CERN lead beam program, arXiv:nucl-th/0002042.

[2] M. Ruggieri, F. Scardina, S. Plumari, and V. Greco, Thermalization, isotropization and elliptic flow from non-equilibrium initial conditions with a saturation scale, Phys. Rev. C **89**, 054914 (2014).

[3] M. Ruggieri, F. Scardina, S. Plumari, and V. Greco, Elliptic flow from non-equilibrium initial condition with a saturation scale, Phys. Lett. B **727**, 177 (2013).

[4] S. Plumari, Anisotropic flows and the shear viscosity of the QGP within an event-by-event massive parton transport approach, Eur. Phys. J. C **79**, 2 (2019).

[5] K. Dusling, W. Li, and B. Schenke, Novel collective phenomena in high-energy proton–proton and proton–nucleus collisions, Int. J. Mod. Phys. E **25**, 1630002 (2016).

[6] A. Kurkela, U. A. Wiedemann, and B. Wu, Opacity dependence of elliptic flow in kinetic theory, Eur. Phys. J. C **79**, 759 (2019).

[7] A. Kurkela, U. A. Wiedemann, and B. Wu, Flow in AA and pA as an interplay of fluid-like and non-fluid like excitations, Eur. Phys. J. C **79**, 965 (2019).

[8] M. Greif, C. Greiner, B. Schenke, S. Schlichting, and Z. Xu, Importance of initial and final state effects for azimuthal correlations in p + Pb collisions, Phys. Rev. D **96**, 091504 (2017).

[9] W. Zhao, S. Ryu, C. Shen, and B. Schenke, 3D structure of anisotropic flow in small collision systems at energies available at the BNL relativistic heavy ion collider, Phys. Rev. C **107**, 014904 (2023).

[10] L. Oliva, W. Fan, P. Moreau, S. A. Bass, and E. Bratkovskaya, Nonequilibrium effects and transverse spherocity in ultrarelativistic proton-nucleus collisions, Phys. Rev. C **106**, 044910 (2022).

[11] L. Oliva, W. Fan, P. Moreau, S. A. Bass, and E. Bratkovskaya, Non-equilibrium dynamics and collectivity in ultra-relativistic proton–nucleus collisions, Acta Phys. Pol. B Proc. Suppl. **16**, 1 (2023).

[12] V. Nugara, V. Greco, and S. Plumari, Far-from-equilibrium attractors with full relativistic Boltzmann approach in 3 + 1D: Moments of distribution function and anisotropic flows v_n, Eur. Phys. J. C **85**, 311 (2025).

[13] J. F. Grosse-Oetringhaus and U. A. Wiedemann, A decade of collectivity in small systems, arXiv:2407.07484.

[14] T. Lappi and L. McLerran, Some features of the glasma, Nucl. Phys. **A772**, 200 (2006).

[15] L. D. McLerran and R. Venugopalan, Computing quark and gluon distribution functions for very large nuclei, Phys. Rev. D **49**, 2233 (1994).

[16] L. D. McLerran and R. Venugopalan, Gluon distribution functions for very large nuclei at small transverse momentum, Phys. Rev. D **49**, 3352 (1994).

[17] L. D. McLerran and R. Venugopalan, Green's functions in the color field of a large nucleus, Phys. Rev. D **50**, 2225 (1994).

[18] F. Gelis, E. Iancu, J. Jalilian-Marian, and R. Venugopalan, The color glass condensate, Annu. Rev. Nucl. Part. Sci. **60**, 463 (2010).

[19] E. Iancu and R. Venugopalan, The color glass condensate and high-energy scattering in QCD, in *Quark-Gluon Plasma 4*, edited by R. C. Hwa and X.-N. Wang (World Scientific, Singapore, 2004), pp. 249–3363.

[20] L. McLerran, A brief introduction to the color glass condensate and the glasma, in *38th International Symposium on Multiparticle Dynamics* (2009), pp. 3–18, arXiv:0812.4989.

[21] F. Gelis, Color glass condensate and glasma, Int. J. Mod. Phys. A **28**, 1330001 (2013).

[22] B. Schenke, P. Tribedy, and R. Venugopalan, Event-by-event gluon multiplicity, energy density, and eccentricities in ultrarelativistic heavy-ion collisions, Phys. Rev. C **86**, 034908 (2012).

[23] B. Schenke, P. Tribedy, and R. Venugopalan, Fluctuating glasma initial conditions and flow in heavy ion collisions, Phys. Rev. Lett. **108**, 252301 (2012).

[24] G. D. Moore and D. Teaney, How much do heavy quarks thermalize in a heavy ion collision?, Phys. Rev. C **71**, 064904 (2005).

[25] H. van Hees, V. Greco, and R. Rapp, Heavy-quark probes of the quark-gluon plasma at RHIC, Phys. Rev. C **73**, 034913 (2006).

[26] H. van Hees, M. Mannarelli, V. Greco, and R. Rapp, Nonperturbative heavy-quark diffusion in the quark-gluon plasma, Phys. Rev. Lett. **100**, 192301 (2008).

[27] P. B. Gossiaux and J. Aichelin, Towards an understanding of the RHIC single electron data, Phys. Rev. C **78**, 014904 (2008).

[28] M. He, R. J. Fries, and R. Rapp, Heavy-quark diffusion and hadronization in quark-gluon plasma, Phys. Rev. C **86**, 014903 (2012).

[29] W. M. Alberico, A. Beraudo, A. De Pace, A. Molinari, M. Monteno, M. Nardi, and F. Prino, Heavy-flavour spectra in high energy nucleus-nucleus collisions, Eur. Phys. J. C **71**, 1666 (2011).

[30] T. Lang, H. van Hees, J. Steinheimer, G. Inghirami, and M. Bleicher, Heavy quark transport in heavy ion collisions at energies available at the BNL relativistic heavy ion collider and at the CERN large hadron collider within the UrQMD hybrid model, Phys. Rev. C **93**, 014901 (2016).

[31] S. K. Das, F. Scardina, S. Plumari, and V. Greco, Heavy-flavor in-medium momentum evolution: Langevin versus Boltzmann approach, Phys. Rev. C **90**, 044901 (2014).

[32] T. Song, H. Berrehrah, D. Cabrera, J. M. Torres-Rincon, L. Tolos, W. Cassing, and E. Bratkovskaya, Tomography of the quark-gluon-plasma by charm quarks, Phys. Rev. C **92**, 014910 (2015).

[33] T. Song, H. Berrehrah, D. Cabrera, W. Cassing, and E. Bratkovskaya, Charm production in Pb + Pb collisions at energies available at the CERN large hadron collider, Phys. Rev. C **93**, 034906 (2016).

[34] S. Cao, G.-Y. Qin, and S. A. Bass, Energy loss, hadronization and hadronic interactions of heavy flavors in relativistic heavy-ion collisions, Phys. Rev. C **92**, 024907 (2015).

[35] A. Andronic *et al.*, Heavy-flavour and quarkonium production in the LHC era: From proton–proton to heavy-ion collisions, Eur. Phys. J. C **76**, 107 (2016).

[36] A. Beraudo, A. De Pace, M. Monteno, M. Nardi, and F. Prino, Heavy-flavour production in high-energy d-Au and p-Pb collisions, J. High Energy Phys. 03 (2016) 123.
[37] S. K. Das, F. Scardina, S. Plumari, and V. Greco, Toward a solution to the R_{AA} and v_2 puzzle for heavy quarks, Phys. Lett. B **747**, 260 (2015).
[38] S. K. Das, M. Ruggieri, S. Mazumder, V. Greco, and J.-e. Alam, Heavy quark diffusion in the pre-equilibrium stage of heavy ion collisions, J. Phys. G **42**, 095108 (2015).
[39] S. K. Das, J. M. Torres-Rincon, L. Tolos, V. Minissale, F. Scardina, and V. Greco, Propagation of heavy baryons in heavy-ion collisions, Phys. Rev. D **94**, 114039 (2016).
[40] S. K. Das, S. Plumari, S. Chatterjee, J. Alam, F. Scardina, and V. Greco, Directed flow of charm quarks as a witness of the initial strong magnetic field in ultra-relativistic heavy ion collisions, Phys. Lett. B **768**, 260 (2017).
[41] S. Cao, T. Luo, G.-Y. Qin, and X.-N. Wang, Linearized Boltzmann transport model for jet propagation in the quark-gluon plasma: Heavy quark evolution, Phys. Rev. C **94**, 014909 (2016).
[42] G. Aarts *et al.*, Heavy-flavor production and medium properties in high-energy nuclear collisions—what next?, Eur. Phys. J. A **53**, 93 (2017).
[43] F. Prino and R. Rapp, Open heavy flavor in QCD matter and in nuclear collisions, J. Phys. G **43**, 093002 (2016).
[44] F. Scardina, S. K. Das, V. Minissale, S. Plumari, and V. Greco, Estimating the charm quark diffusion coefficient and thermalization time from D meson spectra at energies available at the BNL relativistic heavy ion collider and the CERN large hadron collider, Phys. Rev. C **96**, 044905 (2017).
[45] S. K. Das, M. Ruggieri, F. Scardina, S. Plumari, and V. Greco, Effect of pre-equilibrium phase on R_{AA} and v_2 of heavy quarks in heavy ion collisions, J. Phys. G **44**, 095102 (2017).
[46] V. Greco, Heavy flavor production, flow and energy loss, Nucl. Phys. **A967**, 200 (2017).
[47] Y. Xu, J. E. Bernhard, S. A. Bass, M. Nahrgang, and S. Cao, Data-driven analysis for the temperature and momentum dependence of the heavy-quark diffusion coefficient in relativistic heavy-ion collisions, Phys. Rev. C **97**, 014907 (2018).
[48] S. Chatterjee and P. Bożek, Large directed flow of open charm mesons probes the three dimensional distribution of matter in heavy ion collisions, Phys. Rev. Lett. **120**, 192301 (2018).
[49] S. Chatterjee and P. Bozek, Interplay of drag by hot matter and electromagnetic force on the directed flow of heavy quarks, Phys. Lett. B **798**, 134955 (2019).
[50] A. Beraudo *et al.*, Extraction of heavy-flavor transport coefficients in QCD matter, Nucl. Phys. **A979**, 21 (2018).
[51] S. Cao *et al.*, Toward the determination of heavy-quark transport coefficients in quark-gluon plasma, Phys. Rev. C **99**, 054907 (2019).
[52] Y. Xu *et al.*, Resolving discrepancies in the estimation of heavy quark transport coefficients in relativistic heavy-ion collisions, Phys. Rev. C **99**, 014902 (2019).
[53] X. Dong and V. Greco, Heavy quark production and properties of quark–gluon plasma, Prog. Part. Nucl. Phys. **104**, 97 (2019).
[54] T. Song, P. Moreau, J. Aichelin, and E. Bratkovskaya, Exploring non-equilibrium quark-gluon plasma effects on charm transport coefficients, Phys. Rev. C **101**, 044901 (2020).
[55] X. Dong, Y.-J. Lee, and R. Rapp, Open heavy-flavor production in heavy-ion collisions, Annu. Rev. Nucl. Part. Sci. **69**, 417 (2019).
[56] T. Song, P. Moreau, Y. Xu, V. Ozvenchuk, E. Bratkovskaya, J. Aichelin, S. A. Bass, P. B. Gossiaux, and M. Nahrgang, Traces of nonequilibrium effects, initial condition, bulk dynamics, and elementary collisions in the charm observables, Phys. Rev. C **101**, 044903 (2020).
[57] J. Zhao, K. Zhou, S. Chen, and P. Zhuang, Heavy flavors under extreme conditions in high energy nuclear collisions, Prog. Part. Nucl. Phys. **114**, 103801 (2020).
[58] L. Oliva, S. Plumari, and V. Greco, Directed flow of D mesons at RHIC and LHC: Non-perturbative dynamics, longitudinal bulk matter asymmetry and electromagnetic fields, J. High Energy Phys. 05 (2021) 034.
[59] L. Oliva, Electromagnetic fields and directed flow in large and small colliding systems at ultrarelativistic energies, Eur. Phys. J. A **56**, 255 (2020).
[60] A. Beraudo, A. De Pace, M. Monteno, M. Nardi, and F. Prino, Rapidity dependence of heavy-flavour production in heavy-ion collisions within a full $3+1$ transport approach: Quenching, elliptic and directed flow, J. High Energy Phys. 05 (2021) 279.
[61] M. Ruggieri, Pooja, J. Prakash, and S. K. Das, Memory effects on energy loss and diffusion of heavy quarks in the quark-gluon plasma, Phys. Rev. D **106**, 034032 (2022).
[62] Pooja, S. K. Das, V. Greco, and M. Ruggieri, Thermalization and isotropization of heavy quarks in a non-Markovian medium in high-energy nuclear collisions, Phys. Rev. D **108**, 054026 (2023).
[63] Y. Sun, S. Plumari, and S. K. Das, Exploring the effects of electromagnetic fields and tilted bulk distribution on directed flow of D mesons in small systems, Phys. Lett. B **843**, 138043 (2023).
[64] S. K. Das, J. M. Torres-Rincon, and R. Rapp, Charm and bottom hadrons in hot hadronic matter, Phys. Rep. **1129–1131**, 1 (2025).
[65] J. a. Barata, S. Hauksson, X. Mayo López, and A. V. Sadofyev, Jet quenching in the glasma phase: Medium-induced radiation, Phys. Rev. D **110**, 094055 (2024).
[66] S. Mrowczynski, Heavy quarks in turbulent QCD plasmas, Eur. Phys. J. A **54**, 43 (2018).
[67] M. Ruggieri and S. K. Das, Cathode tube effect: Heavy quarks probing the glasma in p-Pb collisions, Phys. Rev. D **98**, 094024 (2018).
[68] Y. Sun, G. Coci, S. K. Das, S. Plumari, M. Ruggieri, and V. Greco, Impact of glasma on heavy quark observables in nucleus-nucleus collisions at LHC, Phys. Lett. B **798**, 134933 (2019).
[69] J. H. Liu, S. Plumari, S. K. Das, V. Greco, and M. Ruggieri, Diffusion of heavy quarks in the early stage of high-energy nuclear collisions at energies available at the BNL relativistic heavy ion collider and at the CERN large hadron collider, Phys. Rev. C **102**, 044902 (2020).
[70] J.-H. Liu, S. K. Das, V. Greco, and M. Ruggieri, Ballistic diffusion of heavy quarks in the early stage of relativistic

heavy ion collisions at RHIC and the LHC, Phys. Rev. D **103**, 034029 (2021).
[71] K. Boguslavski, A. Kurkela, T. Lappi, and J. Peuron, Heavy quark diffusion in an overoccupied gluon plasma, J. High Energy Phys. 09 (2020) 077.
[72] M. E. Carrington, A. Czajka, and S. Mrowczynski, Heavy quarks embedded in glasma, Nucl. Phys. **A1001**, 121914 (2020).
[73] A. Ipp, D. I. Müller, and D. Schuh, Jet momentum broadening in the pre-equilibrium glasma, Phys. Lett. B **810**, 135810 (2020).
[74] P. Khowal, S. K. Das, L. Oliva, and M. Ruggieri, Heavy quarks in the early stage of high energy nuclear collisions at RHIC and LHC: Brownian motion versus diffusion in the evolving glasma, Eur. Phys. J. Plus **137**, 307 (2022).
[75] M. E. Carrington, A. Czajka, and S. Mrowczynski, Jet quenching in glasma, Phys. Lett. B **834**, 137464 (2022).
[76] Pooja, S. K. Das, V. Greco, and M. Ruggieri, Anisotropic fluctuations of angular momentum of heavy quarks in the Glasma, Eur. Phys. J. Plus **138**, 313 (2023).
[77] M. E. Carrington, A. Czajka, and S. Mrowczynski, Transport of hard probes through glasma, Phys. Rev. C **105**, 064910 (2022).
[78] S. K. Das *et al.*, Dynamics of hot QCD matter—current status and developments, Int. J. Mod. Phys. E **31**, 12 (2022).
[79] K. Boguslavski, A. Kurkela, T. Lappi, F. Lindenbauer, and J. Peuron, Heavy quark diffusion coefficient in heavy-ion collisions via kinetic theory, Phys. Rev. D **109**, 014025 (2024).
[80] D. Avramescu, V. Băran, V. Greco, A. Ipp, D. I. Müller, and M. Ruggieri, Simulating jets and heavy quarks in the glasma using the colored particle-in-cell method, Phys. Rev. D **107**, 114021 (2023).
[81] H. Pandey, S. Schlichting, and S. Sharma, Heavy-quark momentum broadening in a non-Abelian plasma away from thermal equilibrium, Phys. Rev. Lett. **132**, 222301 (2024).
[82] K. Boguslavski, A. Kurkela, T. Lappi, F. Lindenbauer, and J. Peuron, Jet momentum broadening during initial stages in heavy-ion collisions, Phys. Lett. B **850**, 138525 (2024).
[83] D. Avramescu, V. Greco, T. Lappi, H. Mäntysaari, and D. Müller, The impact of glasma on heavy flavor azimuthal correlations and spectra, Phys. Rev. D **111**, 074036 (2025).
[84] D. Avramescu, V. Greco, T. Lappi, H. Mäntysaari, and D. Müller, Heavy flavor angular correlations as a direct probe of the glasma, Phys. Rev. Lett. **134**, 172301 (2025).
[85] T. Matsui and H. Satz, J/ψ suppression by quark-gluon plasma formation, Phys. Lett. B **178**, 416 (1986).
[86] S. Datta, F. Karsch, P. Petreczky, and I. Wetzorke, Behavior of charmonium systems after deconfinement, Phys. Rev. D **69**, 094507 (2004).
[87] Y. Burnier, M. Laine, and M. Vepsalainen, Quarkonium dissociation in the presence of a small momentum space anisotropy, Phys. Lett. B **678**, 86 (2009).
[88] N. Brambilla, M. A. Escobedo, J. Ghiglieri, and A. Vairo, Thermal width and gluo-dissociation of quarkonium in pNRQCD, J. High Energy Phys. 12 (2011) 116.
[89] P. K. Srivastava, M. Mishra, and C. P. Singh, Color screening scenario for quarkonia suppression in a quasiparticle model compared with data obtained from experiments at the CERN SPS, BNL RHIC, and CERN LHC, Phys. Rev. C **87**, 034903 (2013).
[90] J. Casalderrey-Solana, Dynamical quarkonia suppression in a QGP-brick, J. High Energy Phys. 03 (2013) 091.
[91] N. Brambilla, M. A. Escobedo, J. Ghiglieri, and A. Vairo, Thermal width and quarkonium dissociation by inelastic parton scattering, J. High Energy Phys. 05 (2013) 130.
[92] C. R. Singh, P. K. Srivastava, S. Ganesh, and M. Mishra, Unified description of charmonium suppression in a quark-gluon plasma medium at RHIC and LHC energies, Phys. Rev. C **92**, 034916 (2015).
[93] N. Brambilla, M. A. Escobedo, J. Soto, and A. Vairo, Quarkonium suppression in heavy-ion collisions: An open quantum system approach, Phys. Rev. D **96**, 034021 (2017).
[94] T. Song, J. Aichelin, and E. Bratkovskaya, Production of primordial J/ψ in relativistic $p+p$ and heavy-ion collisions, Phys. Rev. C **96**, 014907 (2017).
[95] Y. Akamatsu, Quarkonium in quark–gluon plasma: Open quantum system approaches re-examined, Prog. Part. Nucl. Phys. **123**, 103932 (2022).
[96] X. Yao, Open quantum systems for quarkonia, Int. J. Mod. Phys. A **36**, 2130010 (2021).
[97] M. He, B. Wu, and R. Rapp, Collectivity of J/ψ mesons in heavy-ion collisions, Phys. Rev. Lett. **128**, 162301 (2022).
[98] T. Miura, Y. Akamatsu, M. Asakawa, and Y. Kaida, Simulation of Lindblad equations for quarkonium in the quark-gluon plasma, Phys. Rev. D **106**, 074001 (2022).
[99] D. Y. A. Villar, J. Zhao, J. Aichelin, and P. B. Gossiaux, New microscopic model for J/ψ production in heavy ion collisions, Phys. Rev. C **107**, 054913 (2023).
[100] N. Brambilla, M. A. Escobedo, A. Islam, M. Strickland, A. Tiwari, A. Vairo, and P. Vander Griend, Heavy quarkonium dynamics at next-to-leading order in the binding energy over temperature, J. High Energy Phys. 08 (2022) 303.
[101] T. Song, J. Aichelin, J. Zhao, P. B. Gossiaux, and E. Bratkovskaya, Bottomonium production in pp and heavy-ion collisions, Phys. Rev. C **108**, 054908 (2023).
[102] T. Song, J. Aichelin, and E. Bratkovskaya, Charmonium production in a thermalizing heat bath, Phys. Rev. C **107**, 054906 (2023).
[103] N. Brambilla, T. Magorsch, M. Strickland, A. Vairo, and P. Vander Griend, Bottomonium suppression from the three-loop QCD potential, Phys. Rev. D **109**, 114016 (2024).
[104] Y. Bai and B. Chen, Probing QGP droplets with charmonium in high-multiplicity proton–proton collisions, Eur. Phys. J. C **84**, 1193 (2024).
[105] S. Delorme, R. Katz, T. Gousset, P. B. Gossiaux, and J.-P. Blaizot, Quarkonium dynamics in the quantum Brownian regime with non-Abelian quantum master equations, J. High Energy Phys. 06 (2024) 060.
[106] X. Du and R. Rapp, Sequential regeneration of charmonia in heavy-ion collisions, Nucl. Phys. **A943**, 147 (2015).
[107] X. Du, M. He, and R. Rapp, Color screening and regeneration of bottomonia in high-energy heavy-ion collisions, Phys. Rev. C **96**, 054901 (2017).
[108] X. Du and R. Rapp, In-medium charmonium production in proton-nucleus collisions, J. High Energy Phys. 03 (2019) 015.

[109] L. Yan, P. Zhuang, and N. Xu, Competition between J/ψ suppression and regeneration in quark-gluon plasma, Phys. Rev. Lett. **97**, 232301 (2006).
[110] K. Zhou, N. Xu, Z. Xu, and P. Zhuang, Medium effects on charmonium production at ultrarelativistic energies available at the CERN large hadron collider, Phys. Rev. C **89**, 054911 (2014).
[111] A. Rothkopf, Heavy quarkonium in extreme conditions, Phys. Rep. **858**, 1 (2020).
[112] A. Andronic *et al.*, Comparative study of quarkonium transport in hot QCD matter, Eur. Phys. J. A **60**, 88 (2024).
[113] Pooja, M. Y. Jamal, P. P. Bhaduri, M. Ruggieri, and S. K. Das, $c\bar{c}$ and $b\bar{b}$ suppression in the glasma, Phys. Rev. D **110**, 094018 (2024).
[114] S. K. Wong, Field and particle equations for the classical Yang-Mills field and particles with isotopic spin, Nuovo Cimento A **65**, 689 (1970).
[115] U. W. Heinz, Quark—gluon transport theory I. The classical theory, Ann. Phys. (N.Y.) **161**, 48 (1985).
[116] V. Greco, C. M. Ko, and P. Levai, Parton coalescence and anti-proton/pion anomaly at RHIC, Phys. Rev. Lett. **90**, 202302 (2003).
[117] R. J. Fries, B. Muller, C. Nonaka, and S. A. Bass, Hadronization in heavy ion collisions: Recombination and fragmentation of partons, Phys. Rev. Lett. **90**, 202303 (2003).
[118] V. Greco, C. M. Ko, and P. Levai, Parton coalescence at RHIC, Phys. Rev. C **68**, 034904 (2003).
[119] R. J. Fries, B. Muller, C. Nonaka, and S. A. Bass, Hadron production in heavy ion collisions: Fragmentation and recombination from a dense parton phase, Phys. Rev. C **68**, 044902 (2003).
[120] V. Greco, C. M. Ko, and R. Rapp, Quark coalescence for charmed mesons in ultrarelativistic heavy ion collisions, Phys. Lett. B **595**, 202 (2004).
[121] S. Plumari, V. Minissale, S. K. Das, G. Coci, and V. Greco, Charmed hadrons from coalescence plus fragmentation in relativistic nucleus-nucleus collisions at RHIC and LHC, Eur. Phys. J. C **78**, 348 (2018).
[122] T. Lappi, Small x physics and RHIC data, Int. J. Mod. Phys. E **20**, 1 (2011).
[123] B. Schenke, C. Shen, and P. Tribedy, Running the gamut of high energy nuclear collisions, Phys. Rev. C **102**, 044905 (2020).
[124] A. H. Rezaeian, M. Siddikov, M. Van de Klundert, and R. Venugopalan, Analysis of combined HERA data in the impact-parameter dependent saturation model, Phys. Rev. D **87**, 034002 (2013).
[125] C.-N. Yang and R. L. Mills, Conservation of isotopic spin and isotopic gauge invariance, Phys. Rev. **96**, 191 (1954).
[126] A. Krasnitz and R. Venugopalan, Nonperturbative computation of gluon minijet production in nuclear collisions at very high-energies, Nucl. Phys. **B557**, 237 (1999).
[127] K. Fukushima and F. Gelis, The evolving glasma, Nucl. Phys. **A874**, 108 (2012).
[128] M. Ruggieri and S. K. Das, Diffusion of charm and beauty in the glasma, EPJ Web Conf. **192**, 00017 (2018).
[129] M. Y. Jamal, S. K. Das, and M. Ruggieri, Energy loss versus energy gain of heavy quarks in a hot medium, Phys. Rev. D **103**, 054030 (2021).
[130] Y. Sun, G. Coci, S. K. Das, S. Plumari, M. Ruggieri, and V. Greco, Impact of glasma on heavy quark R_{AA} and v_2 in nucleus-nucleus collisions at LHC, Nucl. Phys. **A1005**, 121913 (2021).
[131] J. Zhao, P. B. Gossiaux, T. Song, E. Bratkovskaya, and J. Aichelin, Wigner density approach to quarkonium production in high energy pp collisions, Nuovo Cimento Soc. Ital. Fis. **48**, 5 (2025).
[132] V. Minissale, S. Plumari, Y. Sun, and V. Greco, Multi-charmed and singled charmed hadrons from coalescence: Yields and ratios in different collision systems at LHC, Eur. Phys. J. C **84**, 228 (2024).
[133] M. Cacciari, S. Frixione, N. Houdeau, M. L. Mangano, P. Nason, and G. Ridolfi, Theoretical predictions for charm and bottom production at the LHC, J. High Energy Phys. 10 (2012) 137.
[134] B. B. Abelev *et al.* (ALICE Collaboration), Beauty production in pp collisions at $\sqrt{s} = 2.76$ TeV measured via semi-electronic decays, Phys. Lett. B **738**, 97 (2014).
[135] https://drive.google.com/drive/folders/1qZJA3kvgC12zcapM8fCv1PTS_btS2AqR?usp=sharing.